Superlattices and Microstructures 44 (2008) 137–142

Contents lists available at ScienceDirect

Superlattices and Microstructures

journal homepage: www.elsevier.com/locate/superlattices

Effects of annealing temperature on morphologies and optical properties of ZnO nanostructures

Jinghai Yang [a,b,*], Ming Gao [a], Yongjun Zhang [a], Lili Yang [a], Jihui Lang [a], Dandan Wang [b], Huilian Liu [b,a], Yanqing Liu [a], Yaxin Wang [a], Hougang Fan [a]

[a] *The Institute of Condensed State Physics, Jilin Normal University, Siping, 136000, People's Republic of China*

[b] *Key Laboratory of Excited State Processes, Changchun Institute of Optics, Fine Mechanics and Physics, Chinese Academy of Sciences, Changchun, 130033, People's Republic of China*

ARTICLE INFO

Article history:
Received 7 July 2007
Received in revised form
12 April 2008
Accepted 16 April 2008
Available online 20 June 2008

Keywords:
ZnO nanostructures
Sol–gel method
Optical properties

ABSTRACT

The effects of annealing temperature on the morphologies and optical properties of ZnO nanostructures synthesized by sol–gel method were investigated in detail. The SEM results showed that uniform ZnO nanorods formed at 900 °C. The PL results showed an ultraviolet emission peak and a relatively broad visible light emission peak for all ZnO nanostructures sintered at different temperature. The increase of the crystal size and decrease of tensile stress resulted in the UV emission peak shifted from 386 to 389 nm when annealing temperature rose from 850 to 1000 °C. The growth mechanism of the ZnO nanorods is discussed.

© 2008 Elsevier Ltd. All rights reserved.

1. Introduction

For several years, the versatile II–VI material ZnO has been used in a variety of applications such as gas sensors, surface acoustic wave devices, varistors, piezoelectric transducers, window material for displays and solar cells. In addition, ZnO nanostructures due to the quantum size effect and to the high surface-to-volume ratio, like nanorods, attracted attention as potential optical components integrated in nanometer sized electronic devices. ZnO nanorods were fabricated and investigated by several groups focusing on laser activities [1–3]. ZnO nanostructures were synthesized by chemical solution deposited [4], physical vapor deposition [5], catalyst-free method [6], metal organic chemical vapor deposition [7], thermal evaporation process [8] and vapor–liquid–solid method [9]. Among

* Corresponding author at: The Institute of Condensed State Physics, Jilin Normal University, Siping, 136000, People's Republic of China. Tel.: +86 434 3290009; fax: +86 434 3294566.
E-mail address: jhyang@jlnu.edu.cn (J. Yang).

0749-6036/$ – see front matter © 2008 Elsevier Ltd. All rights reserved.
doi:10.1016/j.spmi.2008.04.006

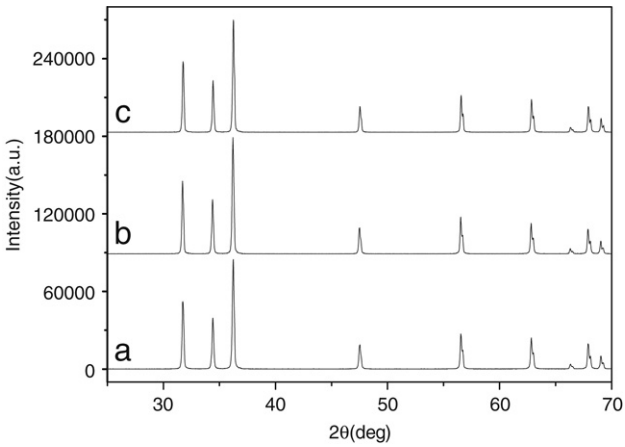

Fig. 1. XRD patterns of samples: (a) annealing at 850 °C; (b) annealing at 900 °C; (c) annealing at 1000 °C.

these techniques the sol–gel method has several advantages. It is easy to carry out, relatively cheap and makes the production of large quantities of materials possible. Thermal annealing was a widely used method to improve crystal quality and to study structural defects in materials. During the annealing process, dislocations and other structural defects moved in the material and adsorption/decomposition would occur on the surface, thus the structure and the stoichiometric ratio of the material would change. Such phenomena had major effects on semiconductor device properties, light emitting devices being particularly affected. For ZnO films, many research groups investigated the effects of annealing temperature on the structure and luminescence properties of ZnO films [10–12]. However, little work focused on the annealing temperature on morphology, structures and photoluminescence of ZnO nanostructures by sol–gel method. In this paper, we report the variation of structural and optical properties of ZnO nanostructures in terms of the thermal annealing conditions and suggest the utility of thermal annealing for the change of various properties of ZnO nanostructures.

2. Experimental

Aqueous solution of zinc nitrate hexahydrate, citric acid and ethylene glycol was first prepared, while keeping at proper molar ratio. All reagents were analytical grade and no further purification was needed. The solution was stirred for 2 h, kept in an oven for some hours to form gel. The gel was kept at 400 °C for 1 h to get amorphous precursor of Zn–C–O composite powers. Then the precursor was put into a box furnace heated to 850 °C, 900 °C and 1000 °C for 13 h respectively. Finally ZnO nanostructures were fabricated by sol–gel methods.

XRD (MAC Science, MXP18, Japan), SEM (Hitachi, S-570) and PL (He–Cd Laser, 325 nm) were used to characterize the crystal structure, surface morphologies and optical properties of ZnO nanostructures.

3. Results and discussion

The XRD patterns showed that all the samples had hexagonal wurtzite structure belong to the C_{6v}^4 space group (*P63mc*) according to the standard JCPDS card (Fig. 1). There were no characteristic peaks from impurities or composite metal oxide. Meanwhile the spectra showed well-defined diffraction peaks which indicated that the samples had perfect crystallization. The grain size of the particles was estimated by the Scherrer formula [13] using FWHM value of the XRD diffraction peaks as follows:

$$D = 0.89\lambda/B\cos\theta \tag{1}$$

where D, λ, θ and B were the grain size, the X-ray wavelength of 0.15604 nm, Bragg diffraction angle and the FWHM of the diffraction peak of the ZnO, respectively. The calculated grain sizes of the

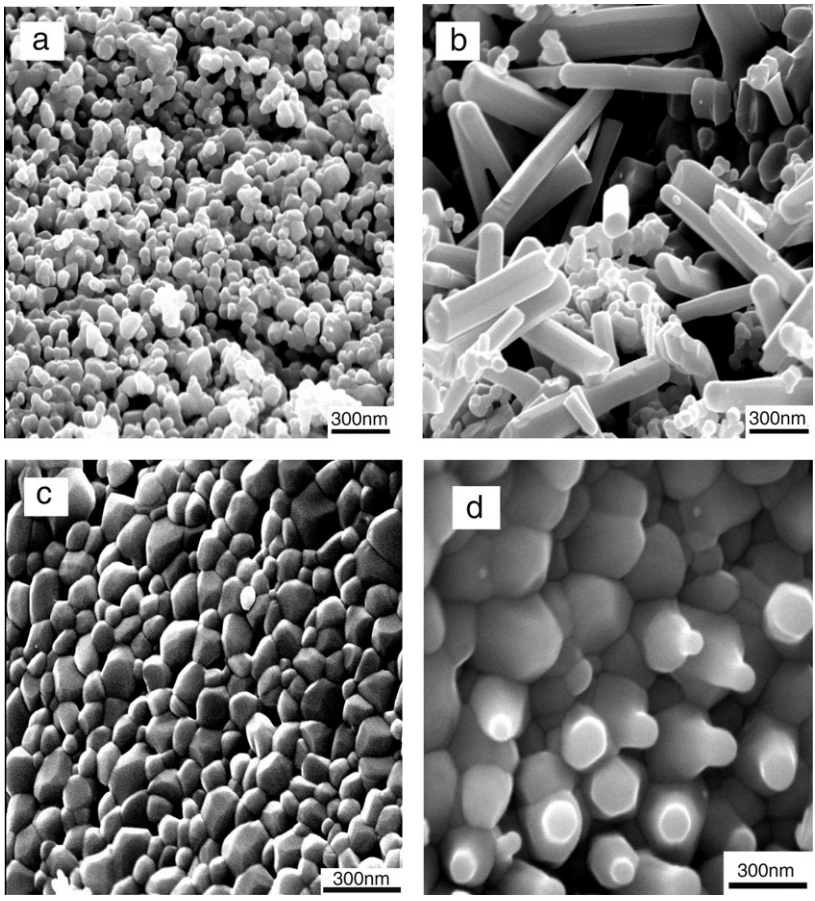

Fig. 2. SEM images of the samples: (a) annealing at 850 °C for 13 h; (b) annealing at 900 °C for 13 h; (c) annealing at 1000 °C for 13 h; (d) annealing at 900 °C for 5 h.

samples sintered at 850 and 1000 °C were 63 and 74 nm respectively, indicating that grain sizes increased with the increasing temperature as also clearly shown by the SEM images (Fig. 2). Moreover, according to Standards JCPDS card, the 2θ angle of the (101) peak for the bulk ZnO without stress was equal to 36.2°. The 2θ angles of the (101) peak for ZnO sintered at 850 and 1000 °C were larger than 36.2°. Thus the tensile stress in our samples changed due to the increase of temperature. We calculated the ZnO stress, using the following formula [14]:

$$\sigma = 450(C_0 - C)/C_0 \text{ GPa} \tag{2}$$

where σ, C and C_0 were the mean stress in the ZnO, lattice constant of ZnO, and lattice constant of bulk ZnO (standard $C_0 = 0.5209$ nm). The calculated stress for the samples sintered at 850 and 1000 °C were equal to 0.13 and 0.108, respectively. It indicated that the tensile stress in ZnO decreased with the increase of temperature from 850 to 1000 °C.

Fig. 2 shows the SEM images of ZnO nanostructures with different annealing temperature of (a) 850 °C, (b) 900 °C and (c) 1000 °C, when the reactive time was fixed at 13 h. But the sample (d) sintered at 900 °C for 5 h. In Fig. 2(b), the sample consisted of a large amount of straight and smooth nanorods with 150–300 nm diameter and 1–2 μm length and less nanoparticles. The annealing temperature had a dominative influence on the microscopic structure and the morphology of ZnO as shown in Fig. 2(a)–(c). As the temperature rose, the ZnO showed different morphologies. In the light of the

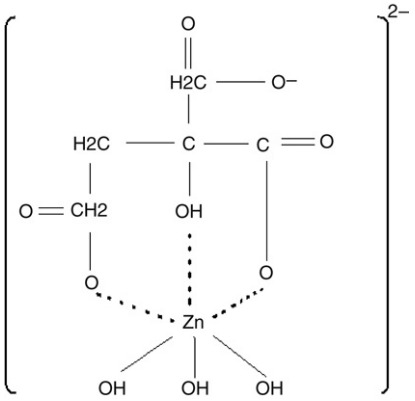

Fig. 3. Schematic illustration of chelate of growth unit.

growth dynamics and the thermodynamics, the higher the temperature, the more disorderly was the particle moved; the high temperature provided the growth of ZnO crystal with the driving force by which the ZnO crystal overcame anisotropic growth. So ZnO was in a granular shape.

Based on the experimental observation, we believed that the growth mechanism of the ZnO nanorod was just as follows:

$$\mathrm{Zn\ (H_2O)_2^{2+}} \rightarrow \mathrm{Zn\ (H_2O)(OH)^{+}} + \mathrm{H^{+}}$$

$$\mathrm{Zn\ (H_2O)(OH)^{+}} \rightarrow \mathrm{Zn\ (OH)_2} \downarrow + \mathrm{H^{+}}$$

$$\mathrm{HO–Zn–OH} + \mathrm{HO–Zn–OH} \rightarrow \mathrm{HO–Zn–O–Zn–OH} + \mathrm{H_2O}$$

$$\mathrm{HO–Zn–O–Zn–OH} + n\mathrm{Zn\ (OH)_2} \rightarrow \mathrm{–O–Zn–O–Zn–O–}.$$

Citric acid as the complexing agent rapidly gathered around the zinc ion, forming two chelate rings as shown in Fig. 3. Under thermal annealing, the zinc hydrogenous and nitrogenous compounds are further decomposed to ZnO, nitrogen oxides and oxygen molecules. When the precursors were annealed, the molecules tended to be perpendicular to the absorbed surface, the growth units would tend to face-land onto the growing interface. Since this kind of landing and dehydration would result in three Zn–O–Zn bonds, which made the face-landing of growing units on axial energetically preferable to both vertex and edge-landing along radial direction. Since the (0 0 1) planes have higher-symmetry (C_{6v}) than the other planes, growing along $+c$-axis was the typical crystal habit. In other words, it was the "lowest-energy" theory [15] that decided the preferential growing plane. The rule was obeyed strictly throughout the process and no branching was observed in single nanorods. In order to prove that the oriented attachment leads to the formation of ZnO nanorods we tried to use the same approach by shorter reactive time. This phenomenon was shown in Fig. 2(d). Fig. 2(d) consisted of nanoparticles and nanorods which only growth a little and would go on upgrowth. Prolonging annealing time at the same temperature would get ZnO nanorods (Fig. 2(b)). Proper annealing time and annealing temperature were important conditions on the growth of ZnO nanorods.

Fig. 4 illustrated the room-temperature PL spectra of the samples sintered at 850 °C, 900 °C and 1000 °C respectively. Two emission bands could be observed from these three samples. One was the near band edge emission at UV range, which was attributed to free-exciton recombination, and the other one was a deep-level emission (DLE) mostly in the green and partly in the yellow and red spectral regions, which was produced by transition of excited optical center from deep level to the valence level, and such deep level emission was usually accompanied by the presence of structural defect and impurities [16,17]. The spectra showed that the positions and intensities of the PL peak were both effected by annealing temperature. In Fig. 4(b), the PL peak in the UV region increased, but the visible emissions decreased. It might be explained the samples would have more perfect crystallization and low density of defects. Compared Fig. 4(a) and (c), the UV emission peak of the ZnO nanoparticles red shifted from 386 to 389 nm with an increase of annealing temperature from 850 to 1000 °C.

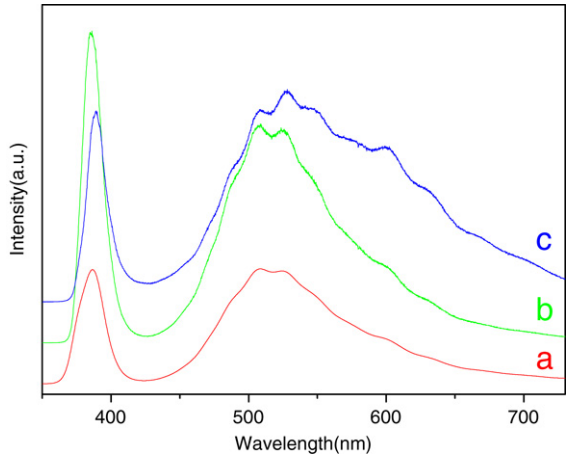

Fig. 4. PL spectrum of samples: (a) ZnO granules obtained at 850 °C, (b) ZnO nanorods obtained at 900 °C, (c) ZnO nanoparticles obtained at 1000 °C.

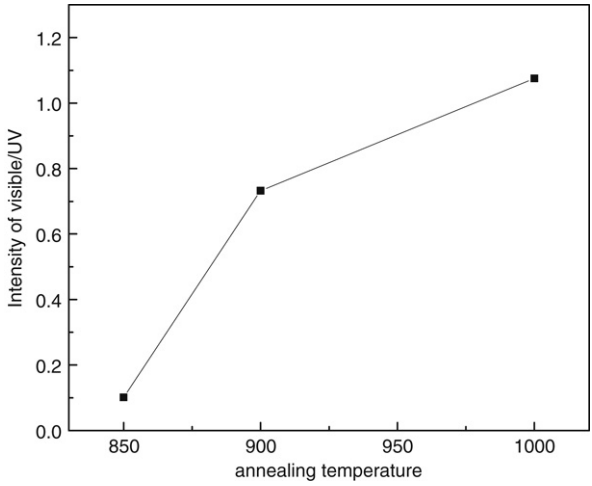

Fig. 5. The intensity ratios between visible and UV luminescence versus annealing temperature.

Quantum confinement effect can not contribute to the red shift of UV peak since the sizes are much larger than the exciton Bohr radius in ZnO [18]. With the increase of annealing temperature, the red shift of band-gap energy was believed to originate from the change of tensile stress due to the lattice distortion. According to XRD analysis, the tensile stress decreased with increasing temperature. If the tensile was released, the band-gap energy was decreased [19]. Various mechanisms have been proposed for the visible light emission of ZnO. Vanheusden et al. found that singly ionized oxygen vacancies (V_{O^+}) are responsible for the green luminescence in the ZnO [20]. Oxygen vacancies occur in three different charge states: the neutral oxygen vacancy (V_{O^+}), the singly ionized oxygen vacancy (V_{O^+}), and the doubly ionized oxygen vacancy ($V_{O^{++}}$) and only the singly ionized oxygen vacancy (V_{O^+}) can act as the so-called luminescent centers [21]. During the annealing process, oxygen is easy to escape from the ZnO nanostructures [22]. Once the concentration of oxygen vacancies increased, the corresponding defect luminescence appears stronger. We plotted the intensity ratios between visible and UV luminescence in Fig. 5. It can be seen for these sample that the visible/UV ratio increases after increasing annealing temperature. This shows that the excitonic luminescence may be suppressed due

to increased defect concentration through trapping or non-radiative recombination at these defect centers [23].

4. Conclusion

In summary, ZnO nanorods could be formed at 900 °C for 13 h by sol–gel method. As the annealing temperature increased, the shape of ZnO nanostructures changed from rod to granule at the same annealing time. The increased temperature led to the redshift of the ultraviolet emission peak. The oriented attachment may be the mechanism of ZnO nanorods growth.

Acknowledgements

This work is supported by the National Natural Science Foundation of China (Grant Nos. 60778040), the Ministry of Science and Technology of China(863) (Item No. 2007AA032400448), the science and technology bureau of Jilin province (Item No. 20060518), gifted youth program of Jilin province (No. 20060123) and the science and technology bureau of Key Program for Ministry of Education (Item No. 207025).

References

[1] M.H. Huang, S. Mao, H. Feick, H. Yan, Y. Wu, H. Kind, E. Weber, R. Russo, P. Yang, Science 292 (2001) 1897.
[2] W.I. Park, Y.H. Jun, S.W. Jung, Gyu-Chul Yi, Appl. Phys. Lett. 82 (2003) 964.
[3] J.C. Johnson, H. Yan, R.D. Schaller, L.H. Haber, R.J. Saykally, P. Yang, J. Phys. Chem. B 105 (2001) 11389.
[4] Jinghai Yang, Jihui Lang, Lili Yang, Yongjun Zhang, Dandan Wang, J. Alloys Comp. (2007), doi:10.1016/j.jallcom.2006.12.135.
[5] Y.C. Kong, D.P. Yu, B. Zhang, W. Fang, S.Q. Feng, Appl. Phys. Lett. 78 (2001) 407.
[6] J.J. Wu, S.C. Liu, J. Phys. Chem. B 106 (2002) 9546; Adv. Mater. 14 (2000) 215.
[7] W.I. Park, D.H. Kim, S.W. Jung, G. Yi, Appl. Phys. Lett. 80 (2002) 4232.
[8] K. Park, J. Lee, M. Sung, S. Kim, Jpn. J. Appl. Phys., Part 1 41 (2002) 7317.
[9] Jinghai Yang, Dandan Wang, Lili Yang, Yongjun Zhang, Jihui Lang, J. Alloys Comp. (2006), doi:10.1016/j.jallcom.2006.11.160.
[10] L. Wang, Y. Pu, W.Q. Fang, J.G. Dai, C.D. Zheng, C.L. Mo, et al., Thin Solid Films 491 (2005) 323.
[11] H.S. Kang, J.S. Kang, S.S. Pang, E.S. Shim, S.Y. Lee, Mater Sci. Eng. B, Solid State Mater Adv. Technol. 102 (2003) 313.
[12] Z.Q. Chen, S. Yamamoto, M. Maekawa, A. Kawasuso, J. Appl. Phys. 94 (2003) 4807.
[13] H.P. Klug, L.E. Alexaander, X-ray Diffraction Procedure for Crystalline and Amorphous Materials, Wiley, New York, 1974, 662.
[14] S. Maniv, W.D. Westwood, E.J. Colombini, Vac. Sci. Technol. 20 (2) (1982) 162.
[15] L. Guo, Y.L. Ji, H.B. Xu, J. Amer. Chem. Soc. 124 (2002) 14864.
[16] P. Zu, Z.K. Tang, G.K.L. Wong, M. Kawasaki, A. Ohtomo, H. Koinuma, Y. Segawa, Solid State Commun. 103 (1997) 459.
[17] D.M. Bagnall, Y.F. Chen, M.Y. Shen, Z. Zhu, T. Goto, T. Yao, J. Cryst. Growth 184–185 (1998) 605.
[18] Gang Xiong, U. Pal, J. Garcia Serrano, J. Appl. Phys. 101 (2007) 024317.
[19] R.J. Hong, J.B. Huang, H.B. He, Z.X. Fan, J.D. Shao, Appl. Surf. Sci. 242 (2005) 346.
[20] K. Vanheusden, W.L. Warren, C.H. Seager, D.R. Tallant, J.A. Voigt, B.E. Gnade, J. Appl. Phys. 79 (1996) 7983.
[21] W. Li, D. Mao, F. Zhang, X. Wang, X. Liu, S. Zou, Y. Zhu, Q. Li, J. Xu, Nuclear Instrum. Methods Phys. Res. B 169 (2000) 59.
[22] L.V. Azaroff, Introduction to Solids, McGraw-Hill, 1960, 371–372.
[23] G. Xiong, U. Pal, J.G. Serrano, K.B. Ucer, R.T. Williams, Phys. Status Solidi C 3 (2006) 3577.